Pergamon

Int. J. Heat Mass Transfer. Vol. 38, No. 17, pp. 3161–3169, 1995

0017-9310/95 $9.50+0.00

0017-9310(95)00061-5

Numerical and experimental analysis of combined convective and radiative heat transfer in laminar flow over a circular cylinder

D. A. KAMINSKI, X. D. FU and M. K. JENSEN

Department of Mechanical Engineering, Aeronautical Engineering and Mechanics, Rensselaer Polytechnic Institute, Troy, NY 12180, U.S.A.

(*Received* 18 *May* 1994 *and in final form* 30 *January* 1995)

Abstract—Flow and heat transfer of a participating medium over a right circular cylinder was investigated experimentally and numerically. Experimental results for the total *Nu* number using combustion products of propane were obtained for Reynolds number 500 and gas temperature up to 1219 K. The length-to-diameter ratio of the cylinder was greater than 10, in order to simulate two-dimensional conditions. A finite-element method was used to solve low Reynolds number flow over a circular cylinder in a radiatively participating medium. Continuity, momentum, energy, and an equation for radiative intensity were solved simultaneously. A constant property assumption allowed decoupling of the momentum and energy equations. The medium was assumed non-gray and non-scattering, and the intensity field was approximated by the P_1 spherical harmonic method for each effective band. Edward's wide band model was used to obtain the absorption coefficient and the effective band width for each band. The average and local Nusselt numbers were calculated for $Re = 500$. The numerical results for the average total *Nu* number are in agreement with the experimental data.

INTRODUCTION

Flow with heat transfer past tube banks is a complex problem of great practical importance. When the fluid is a radiatively participating medium, such as products of combustion, heat transfer occurs by both convection and radiation. The radiation contribution can become significant at high temperatures as, for example, in high-temperature waste heat recovery systems. The thermal and fluid dynamic behavior of a single tube in crossflow yields important insight into flow past banks of tubes.

Experimental results on heat transfer over the circumference of a heated cylinder in transverse flow were published by Schmidt and Wenner [1]. The results included the local heat transfer coefficient on the surface of the cylinder for $5000 < Re < 426\,000$. Eckert and Soehngen [2] successfully performed an experimental study of flow over a cylinder for $20 < Re < 500$, as did Perkins and Leppert [3] for local heat transfer coefficients on a uniformly heated cylinder. The latter results included the local *Nu* number in the range of Reynolds numbers from 2000 to 120 000. Achenbach [4] performed an experimental study for *Re* from 34 000 to 4000 000.

The first successful numerical results for this problem were obtained by Thom [5] for the steady Navier–Stokes (N–S) equations of viscous flow around a cylinder. For unsteady flow, the first results were published by Payne [6] for Reynolds number equal to 40 and 100. More recent simulations of the two-dimensional unsteady N–S equations for flow over a cylinder were developed, for example, by Son and Hanratty [7], Dennis and Chang [8], Loc [9], and Chun and Boehm [10]. Of these, the highest *Re* number was reported by Chun and Boehm who successfully solved this problem with $Re = 3480$. Additionally, Kundu and Haji-Sheikh [11] solved heat transfer in crossflow over cylinders between two parallel plates.

Until now, the main focus in thermal modeling has been on convective heat transfer in the medium range of Reynolds number (2000–200 000). However, the problem of heat transfer at low Reynolds numbers has become increasingly important. At low Reynolds number, very little energy is needed to drive the flow compared with the expenditure on the flow at medium and high Reynolds number.

In the previous work on flow over a cylinder, one important phenomenon has received little attention. When the medium temperature is very high, radiation heat transfer may play an important role in the heat transfer process. For pipe flow and some other internal flows, a considerable body of research has been devoted to the above problem. The results of pipe flow show that radiation can make a large contribution to the total heat transfer [12]. Yang and Ebadian [13] performed a numerical simulation on combined forced convection and radiation for a square duct flow and found that radiation is important when the medium temperature is high. Seo *et al.* [14]

NOMENCLATURE

A_l average band width [μm]
a_{mi} maximum value of the absorption coefficient in Edward's model
a_p Planck mean absorption coefficient, [m^{-1}]
$\bar{a}_{\lambda i}$ spectral absorption coefficient in band i, [m^{-1}]
C_1 parameter in Edward's model [$g^2\ cm^{-1}$]
C_3 parameter in Edward's model [cm^{-1}]
c_p heat capacity [$J\ kg^{-1}\ K^{-1}$]
D diameter of the cylinder, [m]
E_{bi} total effective blackbody emissive power of the gas [$W\ m^{-2}$]
$F_{\lambda i}$ fraction of blackbody total emissive power
H half-width of the test channel [m]
I_0 integrated intensity [$W\ m^{-2}$]
k thermal conductivity, [$W\ m^{-1}\ K^{-1}$]
N conduction to radiation parameter, $\sigma R T_w^3/k$
Nu Nusselt number, $2q_wR/k(T_w-T_i)$
p pressure [Pa]
Pe Peclet number, $Re\ Pr$
Pr Prandtl number, $C_p\mu/k$
q heat flux [$W\ m^{-2}$]
q_c pure convective heat flux, [$W\ m^{-2}$]
q_r radiative heat flux from the cylinder surface to the gas, [$W\ m^{-2}$]
q_w cylinder wall heat flux without surface-to-surface radiation [$W\ m^{-2}$]
R radius of the cylinder [m]
Re Reynolds number, U_0D/ν
T local temperature [K]
T_i inlet temperature [K]
T_w cylinder wall temperature [K]
t time [s]
u local velocity along x axis [$m\ s^{-1}$]
U_0 inlet velocity [$m\ s^{-1}$]
v local velocity along y axis [$m\ s^{-1}$]
x horizontal axis coordinate
y vertical axis coordinate.

Greek symbols
ε_w emissivity of the surface of the cylinder
ε_b emissivity of the surface of the boundary wall
η_i wave number of the absorption band [cm^{-1}]
η_0 wave number of the center of the absorption band [cm^{-1}]
μ dynamic viscosity [$kg\ m^{-1}\ s^{-1}$]
ν kinematic viscosity [$m^2\ s^{-1}$]
σ Stefan–Boltzmann constant [$W\ m^{-2}\ K^{-4}$]
σ_{xx} normal stress, $-p+2\mu\partial u/\partial x$ [Pa]
τ optical thickness
τ_{xy} shear stress, $\mu(\partial u/\partial y)+(\partial v/\partial x)$ [Pa].

Superscripts
* dimensionless quantity, see equation (16).

Subscripts
i for band i, or inlet.

solved for pipe flow using a non-gray model and reported that radiative effects are significant for practical combustion gases.

For external flow the problem of combined convection and radiation of a flow past a sphere has been studied by Jones and Bayazitoglu [15]. Their study indicates that when the Planck number, $k/(4R\sigma T^3)$, is low, radiation heat transfer can dominate the entire process.

In this paper, flow with a Reynolds number of 500 is simulated both numerically and experimentally. Radiative emission and absorption in the fluid is included in the energy equation. In high-temperature heat transfer, (700–1500 K), radiative heat transfer may play an important role in the heat transfer process. This paper is the first to report a combined convective and radiative solution for transient flow over a circular cylinder.

EXPERIMENTS

The test section used to perform the experiments for the present study is shown in Fig. 1. The test section includes a diffuser, flow straightener, test channel, test cylinder, power supply and measurement system. All the experimental data were taken by the data acquisition system and recorded by an IBM 386 PC. Quantities measured include pressure, temperature, flowrate, gas composition and heat flux.

The combustion loop is shown in Fig. 2. Air is heated by combustion of propane. The gas temperature can be controlled by adjusting the flowrate of the injected propane. For each group of experiments, Re was held constant as the gas temperature was raised. The composition of the combustion products was allowed to vary. The difference between the temperatures of the test cylinder surface and incoming

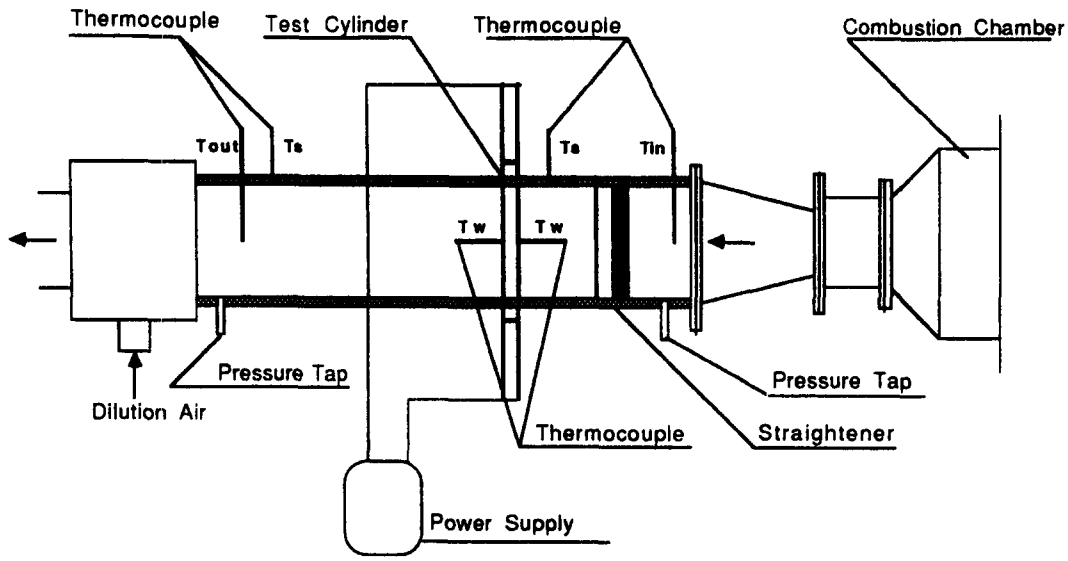

Fig. 1. Schematic diagram of the test section.

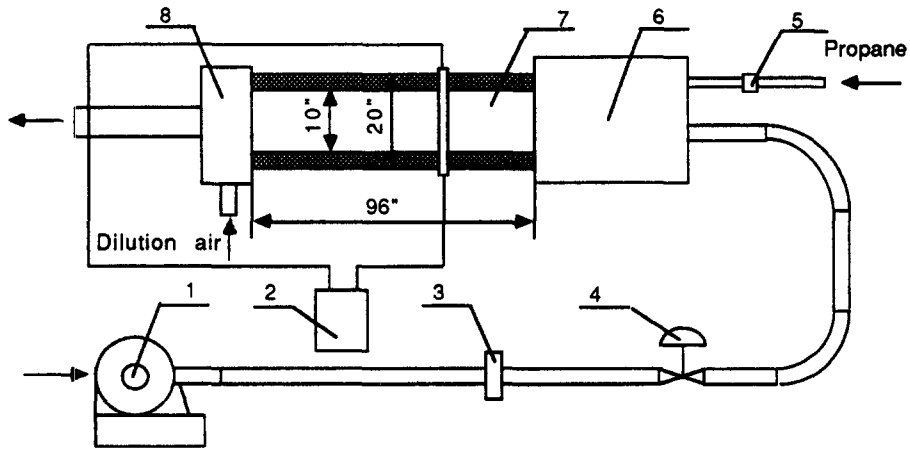

1. Turbine 2. Power Supply 3. Flow Measurement Device
4. Butterfly Valve 5. Rotameter 6. Combustion Chamber
7. Test Section 8. Cooling Section

Fig. 2. Schematic diagram of the experimental combustion loop.

combustion gas was held within the range of 30–45 K.

The test cylinder is made of Inconel, which will withstand temperatures up to 1800 K. Seven K-type thermocouples were installed on the inside surface of the test cylinder and fixed in place by a coaxial cylinder made of Lava. The Lava material, which was obtained from AlsiMag Technical Ceramics Inc., has a unique physical property: when this material is heated to about 800 K, it will expand and take a permanent set. It will not subsequently shrink when it is cooled down. Using this property, a shrink fit was performed between the test cylinder and the Lava rod to fix the thermocouples in place. These seven thermocouples were used to measure the temperature profile along the test cylinder surface.

The thermocouples measuring the inlet and outlet gas temperatures are sheathed by small pieces of honeycomb to prevent thermal radiative losses. Generally, without radiation, two unsheathed thermocouples of different bead size should measure the same temperature. However, if the radiation effect is included, the ratio of convective to radiative heat transfer depends on the bead diameter, and the measured values could be very different [16]. To prove that the radiative effects are reduced, the temperature difference measured by two unsheathed thermocouples of different bead size was compared with

that measured by these two thermocouples sheathed by a honeycomb. When the gas temperature is over 800 K, the two unsheathed thermocouples of different bead size showed a temperature difference of up to 27 K. The sheathed thermocouples showed a much smaller temperature difference of only 7 K. Therefore, the above method substantially reduces radiation effects.

To reduce the cylinder end effects, the ratio of the width of the test channel to the diameter of the cylinder was set at 10. For this geometry, a two-dimensional assumption is reasonable. The cylinder specifications are: 25.4 mm OD; 0.762 mm wall thickness; and 0.46 m length. The channel size is 0.254 m × 0.254 m in cross-section by 1.651 m long and insulated by a 0.102 m ceramic fiber blanket and 25.4 mm high-density ceramic fiber board. The heat loss from the channel to the outside is estimated to be less than 3% of the total heat transfer and can be neglected. The test cylinder was heated by a power supply which can supply up to 2500 A DC. Since the test cylinder wall is machined to a tolerance smaller than 0.025 mm, heat flux is very uniform in the whole tube. Moreover, the ends of the cylinder are insulated by a 50.8 mm thick ceramic fiber blanket to prevent heat loss. The flow straightener consists of a screen and a honeycomb to reduce the turbulence level of the incoming flow in both axial and lateral directions.

Experiments on combined convection and radiation were performed. The space-averaged Nusselt number for convection is defined in the conventional way as:

$$Nu = \frac{q_w D}{k(T_w - T_i)} \tag{1}$$

where

$$q_w = q_r + q_c. \tag{2}$$

The quantity q_r is the surface to gas radiation heat flux from the cylinder to the participating medium, and q_c is the convective heat flux from the cylinder to the gas.

The uncertainty in Nusselt number was estimated to be about 15% based on the accuracy of the thermocouples, the heat conductivity of the gas mixtures, the emissivity of the test cylinder, the uncertainty of the surface to surface radiation, etc. Since the purpose of the present study is the understanding of combined convection and gas radiation, surface to surface radiative heat flux was subtracted from the total heat flux, and is not included in equation (2).

Table 1 shows the measured gas composition for $Re = 500$ at several different values of gas temperature. Gas composition was measured by a Hach Carle Gas Chromatograph (72001-00 Model 01131). The measured results show that propane was completely burned for all of the experiments and the measured gas compositions are close to the theoretical stoichiometric values.

Table 1. The experimental values of the gas compositions

	Gas temp. (K)	CO_2 (%)	H_2O (%)	N_2 (%)	O_2 (%)
Run 1	350	—	—	79.0%	21.0%
Run 2	503	1.1%	1.4%	78.5%	17.2%
Run 3	596	2.1%	2.8%	78.0%	15.4%
Run 4	661	2.3%	3.0%	78.0%	15.2%
Run 5	746	2.6%	3.5%	77.8%	14.6%
Run 6	830	3.4%	4.5%	77.5%	13.3%
Run 7	980	4.3%	5.7%	77.0%	11.7%
Run 8	1061	5.1%	6.8%	76.7%	10.4%
Run 9	1219	6.2%	8.2%	76.2%	8.6%

NUMERICAL ANALYSIS

When *Re* is greater than 9, the flow over a cylinder starts to separate and two vortices are created. If *Re* is greater than 44, the vortices will be shed from the cylinder, and the unsteady N-S and energy equations should be used to study the velocity and temperature fields.

A schematic of the solution domain and the finite-element mesh are shown in Fig. 3. Buoyancy effects are negligible in the present work. Additionally, assuming the ratio of the length to the diameter of the cylinder, L/d, to be greater than 10, the ends of the cylinder can be neglected. Thus, the problem is simplified to two dimensions. The governing equations are:
continuity equation:

$$\frac{\partial u}{\partial x} + \frac{\partial v}{\partial y} = 0 \tag{3}$$

Navier–Stokes equation:

$$\frac{\partial u}{\partial t} + u\frac{\partial u}{\partial x} + v\frac{\partial u}{\partial y} = -\frac{1}{\rho}\frac{\partial p}{\partial x} + \nu\left(\frac{\partial^2 u}{\partial x^2} + \frac{\partial^2 u}{\partial y^2}\right) \tag{4}$$

$$\frac{\partial v}{\partial t} + u\frac{\partial v}{\partial x} + v\frac{\partial v}{\partial y} = -\frac{1}{\rho}\frac{\partial p}{\partial y} + \nu\left(\frac{\partial^2 v}{\partial x^2} + \frac{\partial^2 v}{\partial y^2}\right) \tag{5}$$

the energy equation including radiation:

$$\frac{\partial T}{\partial t} + u\frac{\partial T}{\partial x} + v\frac{\partial T}{\partial y} = \frac{k}{\rho c_p}\left(\frac{\partial^2 T}{\partial x^2} + \frac{\partial^2 T}{\partial y^2}\right) - \nabla \cdot q^r \tag{6}$$

where q^r is the radiative heat flux gradient.

Assuming the medium to be non-gray and non-scattering, the P_1 method [18] was used to model radiative heat transfer for each band. Edward's wide band model [19] was used to estimate the effective band width and the absorption coefficient of each band.

The participating gases are CO_2 and H_2O. According to Edward's wide band model, there are 5 effective bands for CO_2 and 4 effective bands for H_2O. For each band, from Edward's model [20]:

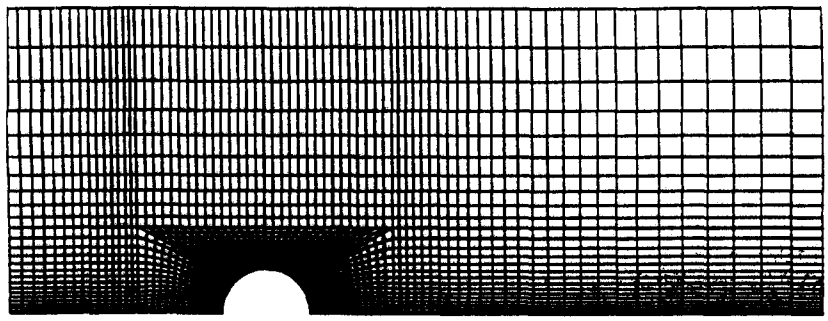

Fig. 3. A schematic diagram of the geometry with finite-element mesh.

$$a_{\lambda i} = C_1/C_3 \exp\left[\frac{(-2|\eta_i - \eta_0|)}{C_3}\right]. \tag{7}$$

From the P_1 equation:

$$\frac{\partial^2 I_{0i}}{\partial x^2} + \frac{\partial^2 I_{0i}}{\partial y^2} = 3\bar{a}_{\lambda i}^2 (I_{0i} - 4E_{bi}) \tag{8}$$

where

$$I_{0i} = \int_{\Delta\lambda i} I_{0\lambda}\, d\lambda \tag{9}$$

$$E_{bi} = \int_{\Delta\lambda i} e_{b\lambda i}\, d\lambda \tag{10}$$

and $\bar{a}_{\lambda i}$ is the average absorption coefficient of each band, which is defined as:

$$\bar{a}_{\lambda i} = \frac{\int_{\Delta\lambda i} a_{\lambda i}(I_{0i} - 4e_{b\lambda i})\, d\lambda}{\int_{\Delta\lambda i}(I_{0\lambda i} - 4e_{b\lambda i})\, d\lambda}. \tag{11}$$

In equation (11), $\bar{a}_{\lambda i}$ cannot be obtained until the integrated intensity, I_{0i}, is known. However, if the assumption that $\bar{a}_{\lambda i} \simeq a_{mi}$ is made, where a_{mi} is the maximum value of the absorption coefficient from equation (7), then a_{mi} can be defined as:

$$a_{mi} = C_1/C_3. \tag{12}$$

Approximating the actual exponential distribution by a top-hat distribution, and setting the area under the two curves equal produces:

$$a_{mi}(\Delta\lambda_m) = \int_{\Delta\lambda i} a_{\lambda i}\, d\lambda. \tag{13}$$

Thus, the absorption coefficient of each band can be approximated by a constant value. For this case, the numerical simulation of a non-gray gas is as simple as that of a gray gas [21].

The Planck mean absorption coefficient predicted using the average value a_{mi} was compared to that predicted from Edward's wide-band model for gas temperature of 1061 K and the conditions shown in Table 1. The results were the same within 2%. Therefore, the above assumption is assumed to be reasonable in the present study, and equation (8) becomes:

$$\frac{\partial^2 I_{0i}}{\partial x^2} + \frac{\partial^2 I_{0i}}{\partial y^2} = 3a_{mi}^2 (I_{0i} - 4E_{bi}). \tag{14}$$

Finally, the integrated form of the equation of transfer is:

$$\nabla \cdot q^r = \sum_{i=1}^{9} a_{mi}(4E_b - I_{0i}) \tag{15}$$

where summation over the nine bands of interest has been made.

Boundary conditions for this problem are: no slip at the surface of the cylinder, uniform incoming flow, symmetric flow above and below the cylinder and no flow stress at the outlet. The thermal boundary conditions are: constant wall temperature, gray diffuse walls and black surroundings at the inlet and outlet.

The symmetric flow assumption was made to save CPU time. Usually, when the *Re* number is not very large, although the flow separates from the cylinder and Von Karman vortices are generated, the time-averaged flow and temperature field can still be approximated as symmetric. Chun and Boehm [10] have shown that this assumption is reasonable for flow with *Re* numbers smaller than 3400.

Introducing the dimensionless variables:

$$x^* = x/R \quad y^* = y/R \quad u^* = u/U_0 \quad v^* = v/U_0$$
$$T^* = T/T_w \quad q^* = q/(T_w k/R) \quad N = \sigma R T_w^3/k$$
$$\tau_i = a_{mi} H \quad I_{0i}^* = I_{0i}/4\sigma T_w^4 \quad p^* = p/\rho U_0^2$$

$$t^* = t/(R/U_0) \tag{16}$$

$$\frac{\partial u^*}{\partial x^*} + \frac{\partial v^*}{\partial y^*} = 0 \tag{17}$$

$$\frac{\partial u^*}{\partial t^*} + u^*\frac{\partial u^*}{\partial x^*} + v^*\frac{\partial u^*}{\partial y^*} = -\frac{\partial p^*}{\partial x^*} + \frac{2}{Re}\left(\frac{\partial^2 u^*}{\partial x^{*2}} + \frac{\partial^2 u^*}{\partial y^{*2}}\right) \tag{18}$$

$$\frac{\partial v^*}{\partial t^*} + u^*\frac{\partial v^*}{\partial x^*} + v^*\frac{\partial v^*}{\partial y^*} = -\frac{\partial p^*}{\partial y^*} + \frac{2}{Re}\left(\frac{\partial^2 v^*}{\partial x^{*2}} + \frac{\partial^2 v^*}{\partial y^{*2}}\right) \tag{19}$$

$$\frac{Pe}{2}\left(\frac{\partial T^*}{\partial t^*}+u^*\frac{\partial T^*}{\partial x^*}+v^*\frac{\partial T^*}{\partial y^*}\right)=\frac{\partial^2 T^*}{\partial x^{*2}}+\frac{\partial^2 T^*}{\partial y^{*2}}+4N\sum_{i=1}^{9}\tau_i[I_{0i}^*-(F_{2\lambda i}-F_{1\lambda i})T^{*4}] \quad (20)$$

$$\frac{\partial^2 I_{0i}^*}{\partial x^{*2}}+\frac{\partial^2 I_{0i}^*}{\partial y^{*2}}=3\tau_i^2[I_{0i}^*-(F_{2\lambda i}-F_{1\lambda i})T^{*4}] \quad (21)$$

and

$$F_{2\lambda i}-F_{1\lambda i}=\frac{E_{bi}}{\sigma T^4}.$$

The Nusselt number in terms of non-dimensional quantities is given by, from equation (1),

$$Nu=\frac{q_w D}{k(T_w-T_i)}=\frac{2q_w^*}{(T_w^*-T_i^*)} \quad (22)$$

where: $q_w^*=q_r^*+q_c^*$. Therefore,

$$Nu=\frac{2q_{wc}^*}{T_w^*-T_i^*}+\frac{4N(\varepsilon_w)\sum_{i=1}^{9}[(F_{2\lambda i}-F_{1\lambda i})-I_{0i}^*]}{(2-\varepsilon_w)(T_w^*-T_i^*)}. \quad (23)$$

Notice that because radiative heat transfer has been included in the total energy equation, this heat transfer coefficient is the total heat transfer coefficient, including both convective and radiative components.

SOLUTION OF THE GOVERNING EQUATIONS

Equations (17)–(21) were solved by the finite-element method. A commercial package, FIDAP, was used to solve the N-S and energy equations. A special purpose code to solve the P_1 approximation was coupled with the FIDAP solution.

For the P_1 approximation, the Galerkin method [22] was used to set up the finite-element equations. Assuming 9 node quadrilateral elements, the shape functions, N_j, can be used to approximate the integrated intensity as:

$$\bar{I}_{0i}^*=\sum_{j=1}^{9}N_j I_{0i,j}^*.$$

Using the shape functions as weighting functions, and integrating the P_1 equation over the solution domain produces:

$$\sum\left(-\int\int_{\Omega}\left(\frac{\partial^2 \bar{I}_{0i}^*}{\partial x^{*2}}+\frac{\partial^2 \bar{I}_{0i}^*}{\partial y^{*2}}+3\tau_i^2((F_{2\lambda i}-F_{1\lambda i})T^{*4}-\bar{I}_{0i}^*)\right)N_k\,d\Omega\right)=0. \quad (24)$$

Equation (24) is the basic equation needed to set up the stiffness matrix. After assembling the stiffness matrix for each element, the total assembled matrix is formed. The boundary conditions are used to modify the matrix, and the linear system of the assembled matrix is solved. Then, this program is coupled with the main program of FIDAP.

The number of elements and nodes of the solution domain are 2310 and 9497, respectively. The size of the smallest elements around the cylinder is 0.0086×0.067. The dimensionless size of the solution domain is 7 in height and 13 in length. To refine the grid, the number of elements and the ratio of the grid size to the diameter of the cylinder were adjusted until grid error was less than 1%. At the initial computation, the non-dimensional time step was 0.4. Then, the non-dimensional time step was changed to 0.04 at 4. After time about 75, a periodic steady state was reached, which was very close to the results reported by Son and Hanratty [7].

Additionally, another calculation was performed which shows that the total Nusselt number of the combined heat transfer is not sensitive to the value of boundary wall emissivity, ε_b. This may indicate that the domain size of the present calculation is sufficiently large to simulate a cylinder in an infinite participating medium.

RESULTS AND DISCUSSION

When the above method is used to solve the system of equations, the program converges very quickly, even though the energy equation is very nonlinear. The Newton–Raphson method is used to handle the nonlinearities. An initial approximation of the flow assuming Stokes flow is used to begin the simulation. For the energy equation, the initial guess is the solution without radiation. On an IBM RS/6000 workstation, each run takes about 6 hours of CPU time.

To verify the code, the momentum and energy equations in the absence of radiation were solved for $Re=500$ under the condition of constant wall temperature. The local Nusselt number along the surface of the cylinder was obtained and compared with that reported by Krall and Eckert [23] and Chun and Boehm [10] as shown in Fig. 4. The deviations are not large. The largest deviations between the present work and the data reported occurred after the flow separated from the cylinder, which may be caused by the symmetric flow field assumption, the big time step, and the coarse mesh (there are some small vortices behind the cylinder).

When radiation is included, the local Nusselt number distribution along the surface of the cylinder is as shown in Fig. 5 at various values of gas temperature. At each gas temperature, the *Re* number was held constant at 500 and the difference between the cylinder wall and inlet temperature was held approximately constant. The air and propane flow rates were adjusted to achieve these conditions. Therefore, each curve represents a different gas composition, as shown in Table 1. The gas radiation properties are dependent on the gas temperature, pressure and composition. The conduction–radiation parameter N is only dependent on the medium temperature. The optical thickness τ is

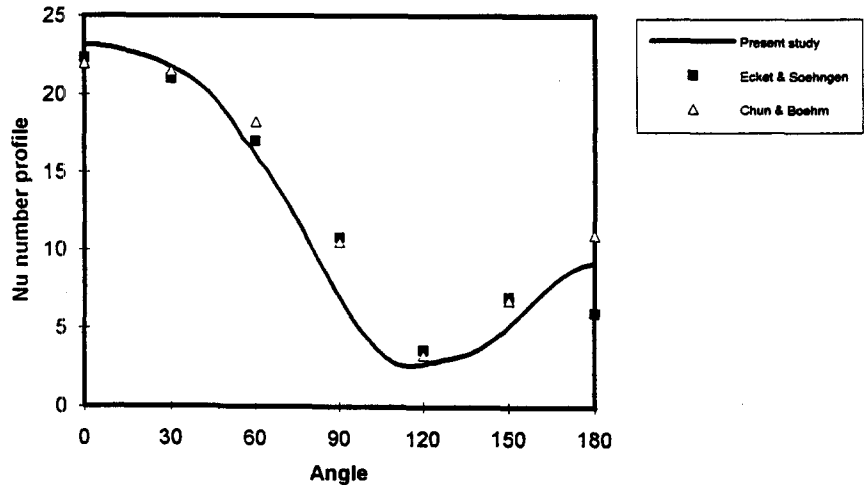

Fig. 4. Local *Nu* profile comparison without radiation.

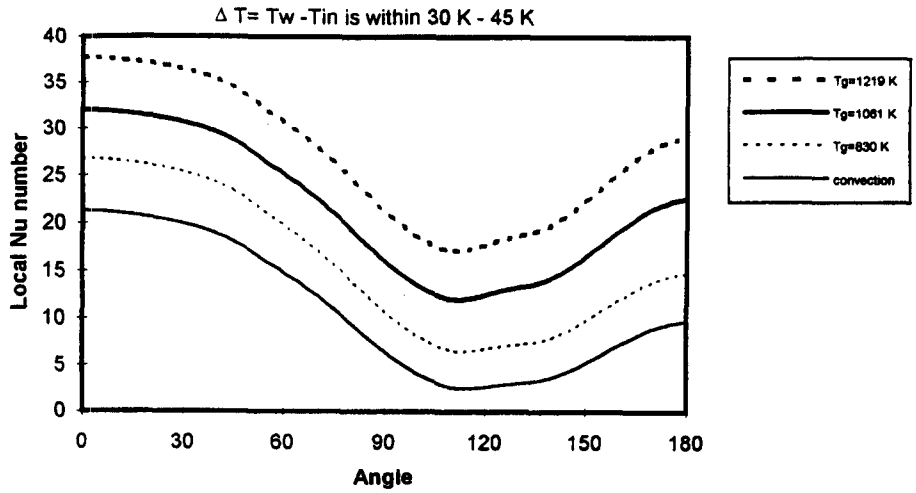

Fig. 5. Local *Nu* profile for different gas temperature. ($\Delta T = T_w - T_{in}$ is within 30–45 K; $Re = 500$.)

dependent on the gas temperature, pressure and composition. Therefore, different gas temperatures imply different magnitudes of N and τ. From Fig. 5, when the gas temperature is 1219 K, the gas radiative effects are significant, even though the percentage of CO_2 and H_2O are less than 10% in the gas. In this case, the total average *Nu* number is about twice as large as that of pure convection.

Figure 6 shows a comparison of the numerical and experimental values of the space-averaged *Nu* number. Good agreement was obtained. The experimental data is a little higher than the numerical simulation, which may be caused by conduction heat losses from the end of the test cylinder and the test channel.

For the same gas composition, the higher the gas temperature, the greater the value of the conduction–radiation parameter N. This implies that the gas radiation increases with gas temperature. Figure 7 shows the numerical *Nu* number vs the location on the surface of the cylinder at different average gas temperatures, but constant gas composition. When the gas temperature is about 746 K, combined radiation and convection is very close to pure convection even though the gas has a high percentage of CO_2 and H_2O. Figure 7 also shows that the total *Nu* number increases quickly with the gas temperature even if gas composition is constant.

The gas composition effects on radiation were predicted by calculating the gas total *Nu* number at the same gas temperature ($T_g = 1219$ K) but different gas compositions. Figure 8 shows the *Nu* number comparison for different mixture gases or different excess air. The *Nu* number does not necessarily increase with the percentage of CO_2 and H_2O. This is because the physical properties of the gas change with gas composition, which can affect the convection. However, when the percentage of CO_2 and H_2O is close to zero, the total *Nu* number of this case approaches that of pure convection.

In Figs. 5, 7 and 8, the shape of the total *Nu* number curve is very similar, which may hint that gas radiation does not strongly affect the convective heat transfer.

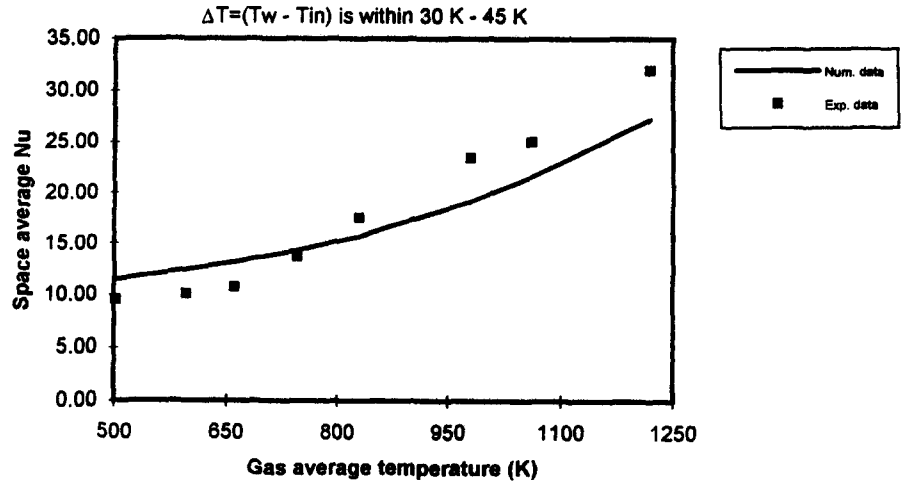

Fig. 6. Space-averaged *Nu* comparison of numerical and experimental data. ($\Delta T = T_w - T_{in}$ is within 30–45 K; $Re = 500$.)

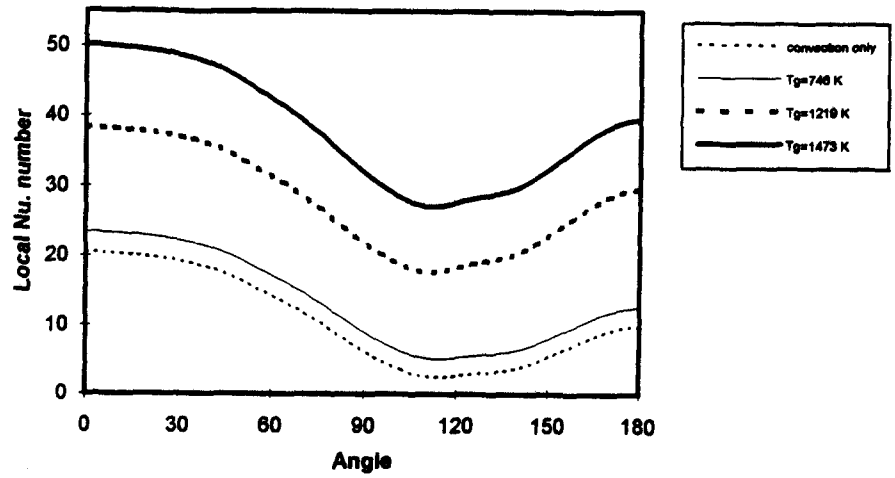

Fig. 7. Local *Nu* for different gas temperature at the same gas composition. (200% of stoichiometric composition, $Re = 500$.)

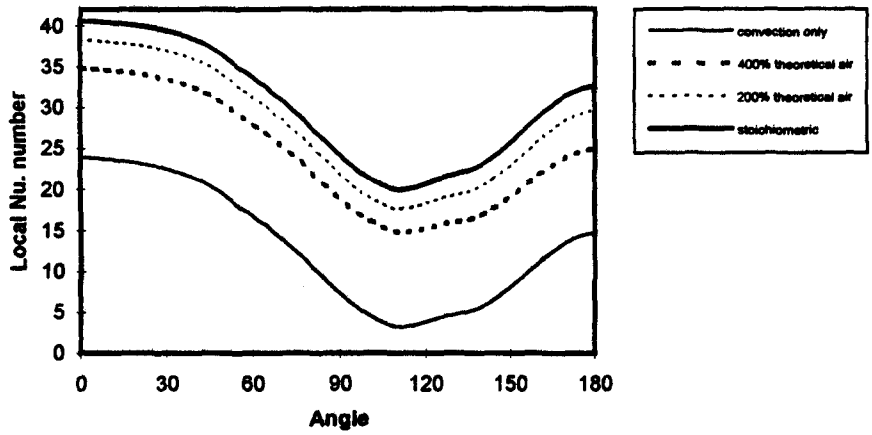

Fig. 8. Local *Nu* for different gas compositions at the same gas temperature. ($\Delta T = T_w - T_{in}$ is within 30–45 K; $Re = 500$; $T_g = 1219$ K.)

However, if the radiative term is much higher than the convective term, this conclusion may not hold. A large radiative heat flux gradient can change the temperature gradient, which will affect the convective heat transfer.

CONCLUSIONS

A transient laminar flow and heat transfer over a circular cylinder has successfully been analysed by both a numerical and experimental technique. Both the momentum and energy equations, including radiation heat transfer were solved by a finite-element method. Radiation in the medium was approximated by the P_1 method for each band. From both the numerical and experimental results, the medium radiative heat transfer does make a significant contribution to the total heat transfer coefficient in low Reynolds number flow. The important factors which can affect the radiative transfer were analysed. In the high-temperature heat transfer case, a small amount of participating gas such as CO_2 and H_2O can bring about significant radiative heat transfer.

REFERENCES

1. E. Schmidt and K. Wenner, Heat transfer over the circumference of a heated cylinder in transverse flow, NACA TM1050 (1941).
2. E. R. G. Eckert and E. Soehngen, Distribution of heat transfer coefficients around circular cylinders in crossflow at Reynolds numbers from 20 to 500, *Trans. ASME* **74,** 343–347 (1952).
3. H. C. Perkins Jr and G. Leppert, Local heat-transfer coefficients on a uniformly heated cylinder, *Int. J. Heat Mass Transfer* **7,** 143–157 (1964).
4. E. Achenbach, Total and local heat transfer from a smooth circular cylinder in cross-flow at high Reynolds number, *Int. J. Heat Mass Transfer* **18,** 1387–1395 (1975).
5. A. Thom, The flow past a circular cylinder at low speeds, *Proc. R. Soc.* A **141,** 651 (1933).
6. R. B. Payne, Calculations of unsteady viscous flow past a circular cylinder, *J. Fluid Mech.* **4,** 81 (1958).
7. J. S. Son and T. J. Hanratty, Numerical solution for flow around a cylinder at Reynolds numbers of 40, 200 and 500, *J. Fluid Mech.* **35,** part 2, 369–386 (1969).
8. S. C. R. Dennis and G. Z. Chang, Numerical solutions for steady flow past a circular cylinder at Reynolds number up to 100, *J. Fluid Mech.* **452,** part 3, 471–489 (1970).
9. Ta Phuoc Loc, Numerical analysis of unsteady secondary vortices generated by an impulsively started circular cylinder, *J. Fluid Mech.* **100,** part 1, 111–128, (1980).
10. W. Chun and R. F. Boehm, Calculation of forced flow and heat transfer around a cylinder in crossflow, *Numer. Heat Transfer* **15,** 101–122 (1989).
11. D. Kundu, A. Haji-Sheikh and D. Y. S. Lou, Pressure and heat transfer in crossflow over cylinder between two parallel plates, *Numer. Heat Transfer, A,* **19,** 345–360 (1990).
12. C. Schuler and A. Campo, Numerical prediction of turbulent heat transfer in gas pipe flows subject to combined convection radiation, *Int. J. Heat Fluid Flow* **9,** 308–315 (1988).
13. G. Yang and M. A. Ebadian, Heat transfer in the entrance region of a square duct considering the effects of turbulent forced convection and radiation, *Radiation Heat Transfer, ASME* **HTD-154,** 41–48 (1990).
14. T. Seo, M. K. Jensen and D. A. Kaminski, Combined convection and non-gray radiation in simultaneously developing flow and heat transfer in internally fined tubes, *10th Int. Heat Transfer Conf.*, Brighton (1994).
15. P. D. Jones and Y. Bayazitoglu, Combined radiation, conduction, and convection from a sphere in an infinite participating medium, *Radiation Heat Transfer, ASME* **HTD-154,** 9–17 (1990).
16. W. H. Giedt and J. T. Chambers, A dual-element transducer for measuring high gas-stream temperatures, ASME publication, 64-WA/HT-45 (1965).
17. X. Fu, Numerical and experimental analysis of combined convective and radiative heat transfer in laminar flow over a circular cylinder, Doctoral Dissertation, Rensselaer Polytechnic Institute (1994).
18. M. F. Modest, *Radiative Heat Transfer*, McGraw-Hill, New York (1993).
19. D. K. Edwards and L. K. Glassen, Radiation heat transfer in non-isothermal nongray gases, *J. Heat Transfer* **89,** 219–228 (1967).
20. R. Siegel and J. R. Howell, *Thermal Radiation Heat Transfer* (2nd Edn). Hemisphere, Washington, DC (1981).
21. D. A. Kaminski and J. P. Moder, A nongray P-N approximation for radiative transfer, *Heat Transfer Phenomena in Radiation, Combustion and Fires,* **HTD-106,** 27–34 (1989).
22. T. J. Chung, *Finite Element Analysis in Fluid Dynamics.* McGraw-Hill, New York (1978).
23. K. M. Krall and E. R. G. Eckert, Heat transfer to transverse circular cylinder at low Reynolds numbers including rarefacting effects, *Heat Transfer* **3,** 225–232 (1970).